Thermoresponsive core-crosslinked nanoparticles from HA-*b*-ELP diblock copolymers

Manon Levêque,[a] Sébastien Lecommandoux,*[a] and Elisabeth Garanger*[a]

AFFILIATIONS

[a] Univ. Bordeaux, CNRS, Bordeaux INP, LCPO, UMR 5629, Pessac, F-33600, France.

ABSTRACT

Stabilization against dilution-dependent disassembly of self-assembled nanoparticles is a requirement for *in vivo* application. Here we propose a simple and biocompatible crosslinking reaction for the stabilization of a series of nanoparticles formed by the self-assembly of amphiphilic HA-*b*-ELP block copolymers, through the alkylation of methionine residues from the ELP block with diglycidyl ether compounds. The core-crosslinked nanoparticles retain their colloïdal properties, with a spherical core-shell morphology, while maintaining thermoresponsive behavior. As such, instead of a reversible disassembly when non-crosslinked, a reversible swelling of nanoparticles' core and increase of hydrodynamic diameter is observed with lowering of the temperature.

KEYWORDS

Elastin-like polypeptides (ELPs), hyaluronan, bioconjugates, thermoresponsiveness, self-assembled nanoparticles, chemoselective crosslinking

INTRODUCTION

Since the end of the 90s, the design and development of efficient nanocarriers for various types of active pharmaceutical ingredients (APIs), such as natural or (hemi)synthetic low molar mass compounds or biologics (*e.g.*, proteins, enzymes, nucleic acids) have been a major field of translational research.[1,2] Nanometer-sized drug delivery systems (DDS) can provide an API with improved solubility, increased stability, stealth properties, and protection against immune system recognition avoiding rapid blood clearance when intravenously injected. In anticancer therapy, DDS limit off-target action of highly cytotoxic drugs and resulting secondary effects, and have often shown in preclinical studies better accumulation in tumors due to longer blood circulation time and the enhanced permeation and retention effect (EPR) as termed by Maeda in 2000 (due to anarchic tumor angiogenesis as already observed by Goldman at the beginning of the 20th century,[3] leaky blood vessels, and deficient lymphatic drainage).[4,5] The EPR effect is however highly controversial since highly tumor- and patient-dependent.[6,7] Specific tumor-targeting strategies have hence emerged to induce the active accumulation of DDS at the tumor site. This can be achieved by decorating the surface of the nanocarriers with ligands able to recognize and bind specific biological receptors overexpressed by tumor cells. The high local concentration of ligands on the nanoparticle can also promote the so-called multivalency effect and trigger specific biological phenomena, such as receptor clustering and activation of signaling cascades.[8–16] If the density of ligands is not compromised *in vivo* when using solid or stable nanoparticles, it can be disrupted when using self-assembled nanoparticles that are formed by intermolecular non-covalent physical interactions between (macro)molecules. The stability of self-assembled nanoparticles is indeed directly linked to concentration, since formed above a critical micellar concentration (CMC) and spontaneously dissociating into soluble unimers below the CMC.[17–19] In other words, upon systemic administration, multivalency of the ligand will be lost by instantaneous dilution of self-assembled NPs below the CMC, and consequently the payload will also be lost prematurely. Stabilization of self-assembled nanocarriers is therefore essential to ensure the conservation of the structural integrity and properties of nanocarriers, and different cross-linking strategies have been proposed, giving rise to different generations of shell cross-linked and core cross-linked micelles.[20–22]

For several years, our group has been particularly interested in the use of elastin-like-polypeptides (ELPs) in particular for the design of self-assembled NPs.[23–29] ELPs are biosynthetic polymers presenting lower critical solution temperature (LCST) phase transition properties in aqueous media.[30–33] Soluble at a specific concentration below the cloud point temperature (T_{cp}), ELP chains hydrophobically collapse above the T_{cp}. Regarding their major assets such as biocompatibility, biodegradability, controlled sequence over synthetic polymers, ease of production in heterologous hosts and purification, ELPs are excellent candidates for the design of self-assembled DDS.[33,34] Fusion of ELP blocks with different LCSTs or conjugation of an ELP to another (macro)molecule can yield macromolecules with controllable amphiphilic character and thermally-driven and reversible self-

assembly or disassembly properties.[35] In some cases however, their use *in vivo* is compromised by their intrinsic lack of stability upon dilution. This has indeed been recently reported both by our group[28] and by the group of Chilkoti.[36] In the latter, fusion proteins made of resilin-like polypeptides (RLPs) and ELPs functionalized at the chain end with a ligand were evidenced to self-assemble into nanoparticles, enabling the multivalent presentation of the ligand. However, a complete loss of efficacy was observed at a concentration below the CMC due to NPs disassembly into unimers. ELPs containing non-natural *para*-azidophenylalanine residues were therefore employed to cross-link NP's core by UV-irradiation. Resulting NPs maintained their binding properties independently of the concentration evidencing their successful colloïdal stabilization with multivalent presentation of the ligand at their surface.

The present work aims at describing a simple way to stabilize self-assembled nanoparticles from hyaluronan-*b*-ELP bioconjugates (HA-*b*-ELP) by the crosslinking of their ELP core. HA was selected to play the dual role of hydrophilic and CD44 receptor-targeting segment.[37–40] CD44 has indeed been shown to be overexpressed at the surface of tumor cells in many cancers,[41–46] and it is considered as a reliable marker for cancerous stem cells (CSCs) that are suspected to be at the origin of tumor relapse after treatment.[47–49] In a previous work, we have described the synthesis of a library of HA-*b*-ELP bioconjugates from the coupling of three cycloalkyne-modified ELP[M_1V_3-n] (n = 60, 80, 100) and three azide-modified hyaluronan of 4.6, 24, and 42 kDa molar mass by strain-promoted azide-alkyne cycloaddition (SPAAC).[28] The phase diagram of the 9 different bioconjugates was established to evidence the domains of temperatures and concentrations where HA-*b*-ELP NPs were stable. Although compatible with biological applications, the results evidenced a necessary cross-linking of NPs' core for subsequent use *in vivo* to avoid the instantaneous disassembly upon systemic administration. To this end, we have taken advantage of the presence of methionine residues in the ELP block whose thioether-containing side chain can be readily modified at acidic pH by halogenoalkane, epoxide, or oxaziridine derivatives.[50–52] As a proof of concept, a series of three HA-*b*-ELP were therefore used, self-assembled and cross-linked using commercial diglycidyl ether compounds. Resulting core-crosslinked NPs were characterized and their response to temperature investigated.

EXPERIMENTAL SECTION

Cross-linking of HA-b-ELP nanoparticles

The procedure used for nanoparticles cross-linking of the three bioconjugates, HA$_{4.6k}$-ELP80, HA$_{24k}$-ELP80 and HA$_{42k}$-ELP80, is identical. The HA-*b*-ELP bioconjugate (0.08 µmol, 1 equiv.) was solubilized in 1 mL of phosphate buffer saline (PBS) acidified with hydrochloric acid (300 mOsm, pH 5). The solution was heated and shacked at 50°C for 10 min in a Thermomixer^{TM} comfort Eppendorf (*ThermoFisher Scientific*) before the addition of hexanediol diglycidyl ether (*BOC Sciences*) (4,93 µmol, 63 equiv., *i.e.*, 6 equiv. per methionine residue). The reaction mixture was kept at 50°C under agitation (800 rpm) for 2 days. It was then purified by dialysis against PBS (300 mOsm, pH 7.4) for 2 days (float-a-lyzer, *Spectra/Por*®, 100 kDa molar mass cut off). The purified solution was finally stored at 4°C. A similar procedure was applied with the resorcinol diglycidyl ether (*Sigma Aldrich*) as cross-linking agent. Monitoring of the cross-linking reactions was achieved by collecting 70 µL of the reaction mixture for dynamic light scattering analysis (DLS) at different time points (t0, *i.e.*, before the addition of crosslinker, 1 h, 7 h, 23 h and 29 h after the addition of crosslinker.)

Size exclusion chromatography (SEC)

SEC analyses were performed on an Ultimate 3000 device (*Thermoscientific*®) equipped with triple detection, including a diode array detector (DAD), a multi-angle light scattering detector (MALS, 18 angles), and a differential refractive index detector (dRI) from Wyatt technology. PBS was used as eluent. The samples were prepared in PBS at a concentration of 2 mg/mL, with ethylene glycol as flow marker. The bioconjugates were separated on Shodex OH Pack KD columns: a first SB G (guard 6*40) followed by two SB 804 HQ (8 * 300) with size exclusion of 5 x 10^3 – 4 x 10^5 g/mol. Measurements were performed at a flowrate of 0.6 mL/min at a pressure of 50 bar and columns temperature was held at 26°C.

Dynamic light scattering (DLS)

DLS measurements were performed on NanoZS instrument (*Malvern*, λ = 633 nm) at a 173° angle at a constant position in the cuvette (constant scattering volume). Quartz cuvettes were used (*Hellma Analytics High Precision Cell with Quartz SUPRASIL,* optical path 3x3 mm) for a volume of 70 µL. The solutions of bioconjugates were prepared in PBS (300 mosm, pH 7.4) at 78 µM. Precise z-average values and size distributions were recorded at temperature below (4-5°C) or above (40-50°C) CMT. The automatic mode recorded 3 measurements of 13-16 runs of 10 sec. The evolutions of derived count rate (DCR) and z-average with temperature were plotted during a heating ramp or cycles of heating-cooling ramps every 2°C.

Stability over time was assessed by DLS measurement at 4°C for solutions of nanoparticles at 78 µM in PBS (300 mosm, pH 7.4) freshly crosslinked and after 1 month storage à 4°C.

Transmission Electron Microscopy (TEM)

TEM imaging was performed at the Bordeaux Imaging Center (BIC) on a Hitachi H7650 microscope (80 kV) equipped with a SC1000 ORIUS 11 Mpx (*GATAN*) camera. The sample of crosslinked nanoparticles of $HA_{4,6k}$-ELP$[M_1V_3$-80] was prepared by dialysis against ultra-pure water of a solution at 78 µM in PBS (300 mosm, pH 7.4). A dilution then assured a concentration of 2.6 µM (0.1 mg/mL). The solution was sprayed on a formvar grid at room temperature and stained with a uranyl acetate solution at 1%.

Cryo Electron Microscopy (CryoEM)

Sample applied to a holey carbon-coated copper grid was plunged into a liquid ethane bath cooled with liquid nitrogen (Leica EMGP). Grids were observed with a Tecnai F20 electron microscope (FEI) operating at 200kV. Images were recorded under low-dose conditions using a 4kx4k FEI Eagle camera.

RESULTS AND DISCUSSION

In the present study, we have focused on three HA-*b*-ELP diblock bioconjugates containing a constant thermosensitive ELP block, namely ELP[M_1V_3-80], and a hydrophilic HA block of variable size, precisely of 4.6, 24 and 42 kDa. In the following, these are referred to as HA$_{4.6k}$-ELP80, HA$_{24k}$-ELP80 and HA$_{42k}$-ELP80, respectively. Their general chemical structure is provided in **Figure 1a**. The method used to stabilize HA-*b*-ELP nanoparticles is sketched on **Figure 1b**. In brief, HA-*b*-ELP bioconjugates were solubilized at 80 μM in phosphate buffer saline (PBS) at pH 5 (to insure sufficient nucleophilicity of the thioether of methionine residues) and heated at 50°C, namely well above their critical micelle temperature (CMT, *i.e.*, from 31 to 36°C depending on the HA block length), to induce their self-assembly into nanometer-sized particles.[28] A diglycidyl ether-containing cross-linking agent was subsequently added to the solution at 50°C and the reaction mixture was left under stirring at this temperature for 2 days to insure efficient intra- and intermolecular cross-linking of methionine residues' side chain within the ELP core of nanoparticles. Hexanediol diglycidyl ether, containing a flexible hexyl chain, was first used as cross-linker, (**Figure 1c**) and an excess of 6 equivalent per methionine residue was found necessary for efficient cross-linking. The temperature applied during the cross-linking reaction insured the HA-*b*-ELP bioconjugate to remain in a self-assembled state. Core cross-linked HA-*b*-ELP nanoparticles were afterwards simply recovered by extensive dialysis against PBS at pH 7.4 to remove the unreacted cross-linker and retrieve a dispersion at physiological pH.
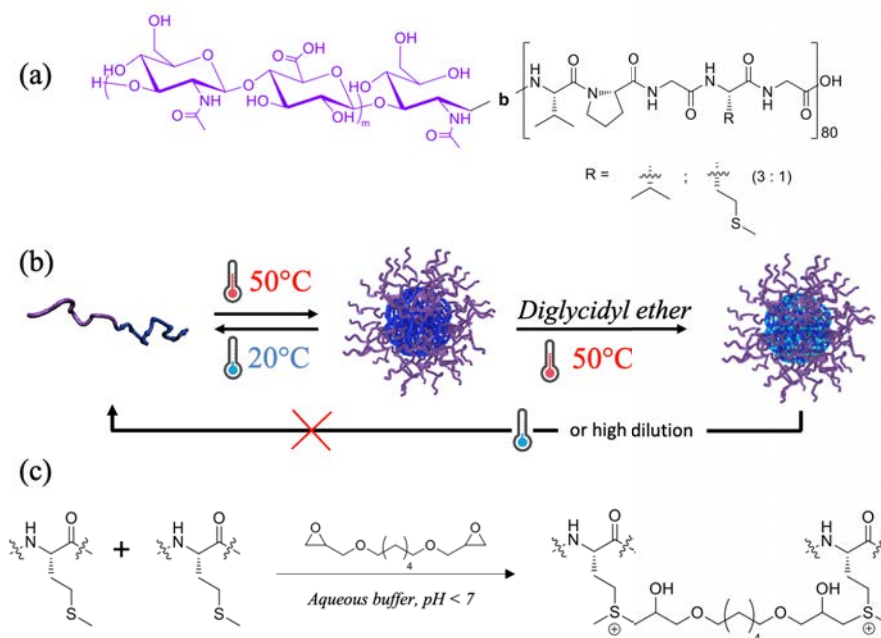

Figure 1. (a) General chemical structure of diblock HA-*b*-ELP bioconjugates. (b) Illustration of the temperature-triggered self-assembly and nanoparticles' core cross-linking step. (c) Synthetic scheme of the crosslinking reaction between methionine residues of the ELP block using hexanediol diglycidyl ether.

The kinetics of the cross-linking reaction was monitored by dynamic light scattering (DLS). Size distributions, expressed in number and intensity, of nano-objects present in solution were plotted at different time points and measured either at 50°C or at 4°C. An example is provided for the HA$_{4.6k}$-ELP80 bioconjugate in **Figure 2** and **S1**. Before addition of the cross-linker (t0), the HA$_{4.6k}$-ELP80 at 50°C (above the CMT) formed 40 nm-sized nanoparticles, (**Figures 2a** and **S1a**) while mainly present as soluble chains (hydrodynamic diameter, D$_H$, of about 10 nm) when the sample was cooled down to 4°C, *i.e.*, below the CMT of the bioconjugate, (**Figures 2b** and **S1b**) in perfect agreement with our previous findings.[28] The polydisperse size distribution, when represented in intensity, (**Figure S1b**) at 4°C is typical of free chains of the bioconjugate in presence of a few aggregates. One hour after the addition of hexanediol diglycidyl ether at 50°C, the situation did not evolve much with well-defined nanoparticles at 50°C, and disassembled nanoparticles upon cooling the sample down to 4°C. However, after one day of reaction (23 and 29 hrs), nanoparticles detected at 50°C were still observed when cooling the sample down to 4°C, implying their inability to disassemble upon cooling. Although the exact cross-ling rate cannot be determined, these results however confirmed indirectly the efficient cross-linking of the ELP chains within the core of nanoparticles. These core crosslinked nanoparticles shall therefore also be stable upon dilution in contrast with non-crosslinked HA-*b*-ELP nanoparticles. It is worth mentioning that, despite their weak nucleophilic character, carboxylic groups from D-glucuronic acid units of HA could also be involved in the crosslinks of nanoparticles. It is however difficult to clearly state on this phenomenon. Zeta potential measurements performed at 50°C on non-crosslinked and crosslinked nanoparticles indeed showed a slightly higher value for crosslinked nanoparticles than the one measured with non-crosslinked nanoparticles. (Data not shown) However, this can result both from the formation of positively charged sulfonium groups (crosslinking through thioether groups) and/or from the loss of carboxylate groups (in case crosslinking occurs through carboxylate groups). Because cross-linked HA-*b*-ELP nanoparticles still recognize and bind to CD44 receptors and CD44-expressing cells (data to be reported elsewhere), we presume few crosslinks in the HA shell of these nanoparticles.
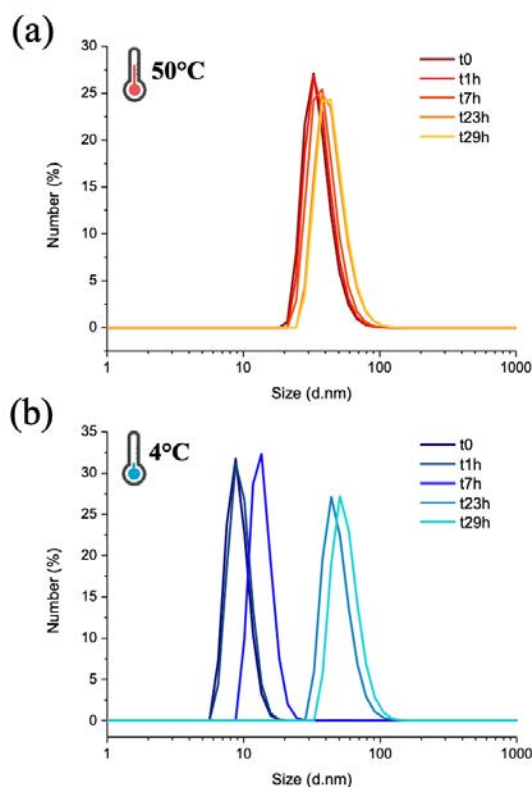
Figure 2. Monitoring of the formation of core crosslinked $HA_{4.6k}$-ELP80 nanoparticles with time during the cross-linking reaction at 50°C. DLS analysis (size distribution expressed in number) of the reaction mixture performed at 50°C (a) and after cooling of the sample at 4°C (b).

Deeper analyses by DLS however showed that core-cross-linked HA-*b*-ELP nanoparticles were still thermally responsive. Indeed, while crosslinked nanoparticles of $HA_{4.6k}$-ELP80 were measured with a 57 nm D_H at 50°C, their hydrodynamic diameter increased up to 87 nm upon cooling at 5°C. (**Figure 3a** and **Table 1**) Interestingly, the decrease in nanoparticle size upon increasing temperature was accompanied with an increase of scattered light intensity as monitored by the derived count rate. (**Figure 3b**) This phenomenon can easily be explained by the different hydration state of ELP chains in the core of nanoparticles at different temperatures. Indeed, in agreement with a previous study by our group,[23] as ELPs gradually desolvate upon increasing temperature, the core of crosslinked $HA_{4.6k}$-ELP80 nanoparticles likely also desolvates and contracts implying an increase in the refractive index increment (dn/dc) and resulting in an increase of the scattered light intensity, that is proportional to $(dn/dc)^2$. Complete aggregation of the ELP in the core of nanoparticle likely occurs well above the measurable temperature range (*i.e.*, > 50°C).

Noteworthily, this phenomenon was found perfectly reversible upon successive heating and cooling ramps. (**Figure 3c**) Nanoparticles from the two other bioconjugates, HA_{24k}-ELP80 and HA_{42k}-ELP80, showed a similar trend. (**Figure S2**) However, the larger the HA block, the smaller the difference in D_H between high and low temperature conditions (*i.e.*, 50 and 5°C). This is consistent with the fact that the larger the HA block, the larger the nanoparticles, and the smaller the proportion of the ELP80 block in

the composition of the bioconjugate. Hydrodynamic size values for all nanoparticles at the two distinct temperatures (5 and 50°C) are summarized in **Table 1**.
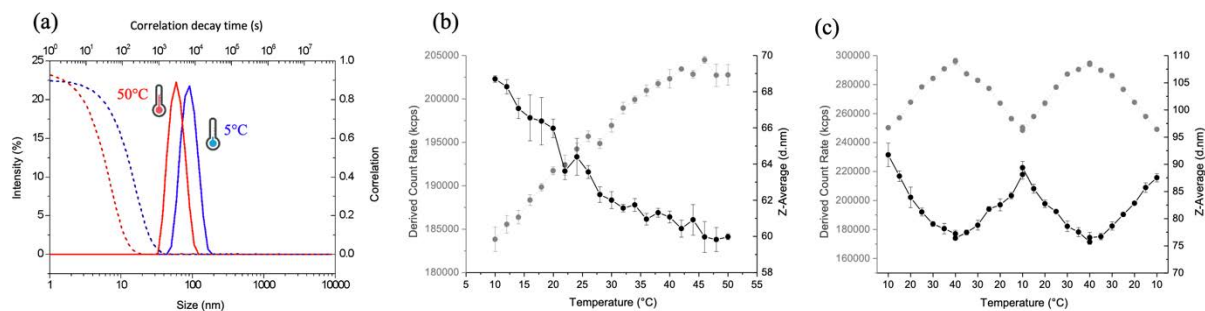

Figure 3. Evidence of the reversible thermal responsiveness of crosslinked HA$_{4.6k}$-ELP80 nanoparticles. (a) DLS analysis (auto-correlation functions represented as doted lines and size distributions expressed in intensity represented as solid lines) of the solution of crosslinked nanoparticles performed at 5°C and 50°C. (b,c) Evolution of the derived count rate (grey, dotted line) and the Z-average (black, solid line) with the temperature for one heating ramp (b) or two cycles of heating and cooling ramps (c).

In the perspective of subsequent biological studies with these nanoparticles, a diblock bioconjugate containing a 5 kDa poly(ethylene glycol) as hydrophilic block instead of a bioactive HA segment was also synthesized, self-assembled and crosslinked to serve as necessary control nanoparticles in these experiments. As expected, core-crosslinked PEG$_{5k}$-ELP80 nanoparticles also showed thermal responsiveness. Although of similar molar mass than the HA$_{4.6k}$-ELP80, self-assembled and crosslinked nanoparticles obtained from the PEG$_{5k}$-ELP80 bioconjugate were found much larger than HA$_{4.6k}$-ELP80 nanoparticles. The difference in D$_H$ for PEG$_{5k}$-ELP80 nanoparticles between 5°C and 50°C is also significantly larger, with an almost doubled size at 5°C.

Table 1. Characteristics of crosslinked HA-ELP80 and PEG-ELP80 nanoparticles.

Diblock copolymer	5°C			50°C			25°C
	D$_h$(nm)	PdI	N	D$_h$(nm)	PdI	N	Zeta Potential (mV)
HA$_{4.6k}$-ELPn80	87 (± 10)	0.17 (± 0.09)	7	57 (± 4)	0.10 (± 0.06)	7	-15.8 (± 0.7)
HA$_{24k}$-ELPn80	114 (± 11)	0.21 (± 0.05)	5	98 (± 10)	0.15 (± 0.03)	6	-22.8 (± 2.5)
HA$_{42k}$-ELPn80	178 (± 38)	0.27 (± 0.04)	5	167 (± 40)	0.21 (± 002)	6	-22.0 (± 2.1)
PEG$_{5k}$-ELPn80	222	0.07	1	119	0.05	1	0.3 (± 0.6)
HA$_{4.6k}$-ELPn80 (resorcinol)	64	0.06	1	59	0.1	1	/

HA$_{4.6k}$-ELP80 nanoparticles were also crosslinked with resorcinol diglycidyl ether containing a benzene ring with low flexibility (**Figure S3**) as compared to the hexyl chain of hexanediol diglycidyl ether. While self-assembled and crosslinked nanoparticles were found of similar size, their thermal responsiveness was almost completely lost. (**Table 1** and **Figure S3**) We assume that this shorter and more rigid crosslinker also able to make Π-Π interactions through the presence of its aromatic ring

results in a tighter crosslinking and a more hydrophobic core nanoparticle core, with low ability for ELP chains to swell and stretch upon solvation at low temperature. Differently formulated, the ELP block crosslinked with resorcinol diglycidyl ether may also have reached complete aggregation.

The zeta potential of these core-crosslinked nanoparticles was also measured and are summarized in **Table 1**. The zeta potential was found negative for all nanoparticles containing a HA block, consistent with the negatively charged carboxylate groups of HA at physiological pH. The zeta potential of PEG_{5k}-ELP80 nanoparticles was in contrast found close to zero in agreement with the neutral PEG block. These results tend to confirm the core-shell structure of nanoparticles, with the ELP in the core and the negatively charged HA or neutral PEG displayed on the surface.

The morphology of these nanoparticles was then confirmed by transmission electron microscopy (TEM) and cryoTEM. The images displayed in **Figure 4** show the conservation of the spherical morphology previously observed for non-crosslinked nanoparticles $HA_{4.6k}$-ELP80,[28] of their nanometric size and monomodal distribution after the crosslinking procedure.

Finally, the stability of nanoparticles over time was assessed by DLS analysis of a solution of nanoparticles freshly crosslinked and after storage in solution at 4°C for one month. (**Figure S4**) The similarity of the size distributions is in favour of a good stability for all the nanoparticles of the series. The stability of nanoparticles with dilution was also confirmed. (**Figure S5**)
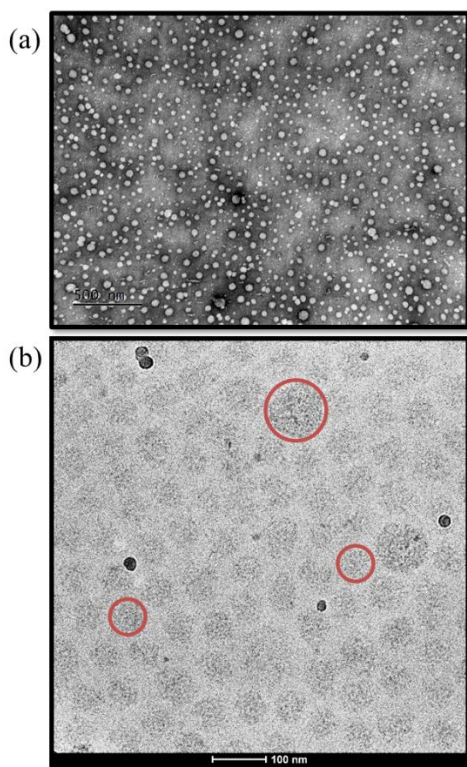

Figure 4. Transmission electron micrographs of crosslinked $HA_{4.6k}$-ELPn80 nanoparticles in pure water. (a) TEM. Sample stained with uranyl acetate. Scale = 500 nm. (b) CryoEM. No stain. Scale = 100 nm. Red circles are used to highlight nanoparticles.

CONCLUSIONS

This work presents the efficient stabilization of a series of self-assembled HA-ELP80 nanoparticles by the crosslinking of the ELP core with diglycidyl ether compounds. This reaction is chemoselective, simple, and compatible with the system and subsequent biological experimentations. The cross-linking does not seem to affect the physicochemical properties of the nanoparticles, which stay spherical with a core-shell structure. The main difference lies in the thermoresponsiveness which goes from a total disassembly of the nanoparticles at low temperature before cross-linking to a mere size variation cross-linking. This variation correlates with the dehydration of the ELP-core at high temperature, leading to its shrinking. This effect is however mitigated by the increase of HA molar mass and the use of a shorter and more hydrophobic crosslinker. In addition with their stability over dilution and temperature, these core-crosslinked nanoparticles also display a good stability over time when stored in solution at low temperature. They seem thus compatible with biological applications, biophysical and *in vitro* cellular experiments being the main topic of a forthcoming publication.

SUPPORTING INFORMATION

SEC chromatograms and additional DLS analyses are available in the supporting information.

AUTHORS INFORMATIONS

Corresponding authors:

garanger@enscbp.fr and lecommandoux@enscbp.fr

Author contributions:

The manuscript was written through contributions of all authors. All authors have given approval to the final version of the manuscript. The authors declare no conflict of interest.

ACKNOWLEDGMENTS

REFERENCES

(1)   Edis, Z.; Wang, J.; Waqas, M. K.; Ijaz, M.; Ijaz, M. Nanocarriers-Mediated Drug Delivery Systems for Anticancer Agents: An Overview and Perspectives. *Int. J. Nanomedicine* **2021**, *Volume 16*, 1313–1330. https://doi.org/10.2147/IJN.S289443.

(2)   Mitchell, M. J.; Billingsley, M. M.; Haley, R. M.; Wechsler, M. E.; Peppas, N. A.; Langer, R. Engineering Precision Nanoparticles for Drug Delivery. *Nat. Rev. Drug Discov.* **2021**, *20* (2), 101–124. https://doi.org/10.1038/s41573-020-0090-8.

(3)   Goldmann, E. The Growth of Malignant Disease in Man and the Lower Animals, with Special Reference to the Vascular System. *Proc. R. Soc. Med.* **1908**, *1* (Surg_Sect), 1–13. https://doi.org/10.1177/003591570800101201.

(4)   Maeda, H.; Wu, J.; Sawa, T.; Matsumura, Y.; Hori, K. Tumor Vascular Permeability and the EPR Effect in Macromolecular Therapeutics: A Review. *J. Control. Release* **2000**, *65* (1–2), 271–284. https://doi.org/10.1016/S0168-3659(99)00248-5.

(5)   Greish, K. Enhanced Permeability and Retention (EPR) Effect for Anticancer Nanomedicine Drug Targeting. *Cancer Nanotechnology* (Springer) **2010**, 25–37. https://doi.org/10.1007/978-1-60761-609-2_3.

(6)   Taurin, S.; Nehoff, H.; Greish, K. Anticancer Nanomedicine and Tumor Vascular Permeability; Where Is the Missing Link? *J. Control. Release* **2012**, *164* (3), 265–275. https://doi.org/10.1016/j.jconrel.2012.07.013.

(7)   de Lázaro, I.; Mooney, D. J. A Nanoparticle's Pathway into Tumours. *Nat. Mater.* **2020**, *19* (5), 486–487. https://doi.org/10.1038/s41563-020-0669-9.

(8)   Kiessling, L. L.; Lamanna, A. C. Multivalency in Biological Systems. *Chemical Probes in Biology* (Springer) **2003**, 345–357. https://doi.org/10.1007/978-94-007-0958-4_26.

(9)   Banerjee, D.; Liu, A. P.; Voss, N. R.; Schmid, S. L.; Finn, M. G. Multivalent Display and Receptor-Mediated Endocytosis of Transferrin on Virus-Like Particles. *ChemBioChem* **2010**, *11* (9), 1273–1279. https://doi.org/10.1002/cbic.201000125.

(10)   Simnick, A. J.; Valencia, C. A.; Liu, R.; Chilkoti, A. Morphing Low-Affinity Ligands into High-Avidity Nanoparticles by Thermally Triggered Self-Assembly of a Genetically Encoded Polymer. *ACS Nano* **2010**, *4* (4), 2217–2227. https://doi.org/10.1021/nn901732h.

(11)   Fasting, C.; Schalley, C. A.; Weber, M.; Seitz, O.; Hecht, S.; Koksch, B.; Dernedde, J.; Graf, C.; Knapp, E. W.; Haag, R. Multivalency as a Chemical Organization and Action Principle. *Angew. Chemie - Int. Ed.* **2012**, *51* (42), 10472–10498. https://doi.org/10.1002/anie.201201114.

(12)   Han, J. H.; Moon, A. R.; Chang, J. H.; Bae, J.; Choi, J. M.; Lee, S. H.; Kim, T.-H. Potentiation of TRAIL Killing Activity by Multimerization through Isoleucine Zipper Hexamerization Motif. *BMB Rep.* **2016**, *49* (5), 282–287. https://doi.org/10.5483/BMBRep.2016.49.5.245.

(13)   Bonduelle, C.; Oliveira, H.; Gauche, C.; Huang, J.; Heise, A.; Lecommandoux, S. Multivalent Effect of Glycopolypeptide Based Nanoparticles for Galectin Binding. *Chem. Commun.* **2016**, *52* (75), 11251–11254. https://doi.org/10.1039/c6cc06437j.

(14)   Sarangthem, V.; Kim, Y.; Singh, T. D.; Seo, B.-Y.; Cheon, S.-H.; Lee, Y.-J.; Lee, B.-H.; Park, R.-W. Multivalent Targeting Based Delivery of Therapeutic Peptide Using AP1-ELP Carrier for Effective Cancer Therapy. *Theranostics* **2016**, *6* (12), 2235–2249. https://doi.org/10.7150/thno.16425.

(15)   Duan, H.; Donovan, M.; Foucher, A.; Schultze, X.; Lecommandoux, S. Multivalent and Multifunctional Polysaccharide-Based Particles for Controlled Receptor Recognition. *Sci. Rep.* **2018**, *8* (1), 1–9. https://doi.org/10.1038/s41598-018-32994-y.

(16)   Wang, J.; Min, J.; Eghtesadi, S. A.; Kane, R. S.; Chilkoti, A. Quantitative Study of the Interaction of Multivalent Ligand-Modified Nanoparticles with Breast Cancer Cells with Tunable Receptor Density. *ACS Nano* **2020**, *14* (1), 372–383. https://doi.org/10.1021/acsnano.9b05689.

(17)   Zhang, C.; Qineng, P.; Zhang, H. Self-Assembly and Characterization of Paclitaxel-Loaded N-Octyl-O-Sulfate Chitosan Micellar System. *Colloids Surfaces B Biointerfaces* **2004**, *39* (1–2), 69–75. https://doi.org/10.1016/j.colsurfb.2004.09.002.

(18)   Xu, J.-P.; Ji, J.; Chen, W.-D.; Shen, J.-C. Novel Biomimetic Polymersomes as Polymer Therapeutics for

Drug Delivery. *J. Control. Release* **2005**, *107* (3), 502–512. https://doi.org/10.1016/j.jconrel.2005.06.013.

(19)   Lu, J.; Owen, S. C.; Shoichet, M. S. Stability of Self-Assembled Polymeric Micelles in Serum. *Macromolecules* **2011**, *44* (15), 6002–6008. https://doi.org/10.1021/ma200675w.

(20)   Read, E. S.; Armes, S. P. Recent Advances in Shell Cross-Linked Micelles. *Chem. Commun.* **2007**, No. 29, 3021. https://doi.org/10.1039/b701217a.

(21)   Talelli, M.; Barz, M.; Rijcken, C. J. F.; Kiessling, F.; Hennink, W. E.; Lammers, T. Core-Crosslinked Polymeric Micelles: Principles, Preparation, Biomedical Applications and Clinical Translation. *Nano Today* **2015**, *10* (1), 93–117. https://doi.org/10.1016/j.nantod.2015.01.005.

(22)   Bauer, T. A.; Schramm, J.; Fenaroli, F.; Siemer, S.; Seidl, C. I.; Rosenauer, C.; Bleul, R.; Stauber, R. H.; Koynov, K.; Maskos, M.; Barz, M. Complex Structures Made Simple – Continuous Flow Production of Core Cross-Linked Polymeric Micelles for Paclitaxel Pro-Drug-Delivery. *Adv. Mater.* **2023**, *35* (21), 2210704–2210712. https://doi.org/10.1002/adma.202210704.

(23)   Garanger, E.; MacEwan, S. R.; Sandre, O.; Brûlet, A.; Bataille, L.; Chilkoti, A.; Lecommandoux, S. Structural Evolution of a Stimulus-Responsive Diblock Polypeptide Micelle by Temperature Tunable Compaction of Its Core. *Macromolecules* **2015**, *48* (18), 6617–6627. https://doi.org/10.1021/acs.macromol.5b01371.

(24)   Le Fer, G.; Portes, D.; Goudounet, G.; Guigner, J. M.; Garanger, E.; Lecommandoux, S. Design and Self-Assembly of PBLG-: B -ELP Hybrid Diblock Copolymers Based on Synthetic and Elastin-like Polypeptides. *Org. Biomol. Chem.* **2017**, *15* (47), 10095–10104. https://doi.org/10.1039/c7ob01945a.

(25)   Le Fer, G.; Wirotius, A. L.; Brûlet, A.; Garanger, E.; Lecommandoux, S. Self-Assembly of Stimuli-Responsive Biohybrid Synthetic- b-Recombinant Block Copolypeptides. *Biomacromolecules* **2019**, *20* (1), 254–272. https://doi.org/10.1021/acs.biomac.8b01390.

(26)   Xiao, Y.; Chinoy, Z. S.; Pecastaings, G.; Bathany, K.; Garanger, E.; Lecommandoux, S. Design of Polysaccharide-b-Elastin-Like Polypeptide Bioconjugates and Their Thermoresponsive Self-Assembly. *Biomacromolecules* **2020**, *21* (1), 114–125. https://doi.org/10.1021/acs.biomac.9b01058.

(27)   Ibrahimova, V.; Zhao, H.; Ibarboure, E.; Garanger, E.; Lecommandoux, S. Thermosensitive Vesicles from Chemically Encoded Lipid-Grafted Elastin-like Polypeptides. *Angew. Chemie Int. Ed.* **2021**, *60* (27), 15036–15040. https://doi.org/10.1002/anie.202102807.

(28)   Levêque, M.; Xiao, Y.; Durand, L.; Massé, L.; Garanger, E.; Lecommandoux, S. Aqueous Synthesis and Self-Assembly of Bioactive and Thermo-Responsive HA-*b*-ELP Bioconjugates. *Biomater. Sci.* **2022**, *10*, 6365–6376. https://doi.org/10.1039/D2BM01149B.

(29)   Grazon, C.; Garanger, E.; Lalanne, P.; Ibarboure, E.; Galagan, J. E.; Grinstaff, M. W.; Lecommandoux, S. Transcription-Factor-Induced Aggregation of Biomimetic Oligonucleotide- b -Protein Micelles. *Biomacromolecules* **2023**, *24* (11), 5027–5034. https://doi.org/10.1021/acs.biomac.3c00662.

(30)   McPherson, D. T.; Morrow, C.; Minehan, D. S.; Wu, J.; Hunter, E.; Urry, D. W. Production and

Purification of a Recombinant Elastomeric Polypeptide, G-(VPGVG)19-VPGV, from Escherichia Coli. *Biotechnol. Prog.* **1992**, *8* (4), 347–352. https://doi.org/10.1021/bp00016a012.

(31)   Urry, D. W. Physical Chemistry of Biological Free Energy Transduction As Demonstrated by Elastic Protein-Based Polymers. *J. Phys. Chem. B* **1997**, *101* (51), 11007–11028. https://doi.org/10.1021/jp972167t.

(32)   Rodríguez-Cabello, J. C.; Martín, L.; Alonso, M.; Arias, F. J.; Testera, A. M. "Recombinamers" as Advanced Materials for the Post-Oil Age. *Polymer (Guildf).* **2009**, *50* (22), 5159–5169. https://doi.org/10.1016/j.polymer.2009.08.032.

(33)   MacEwan, S. R.; Chilkoti, A. Elastin-like Polypeptides: Biomedical Applications of Tunable Biopolymers. *Biopolymers* **2010**, *94* (1), 60–77. https://doi.org/10.1002/bip.21327.

(34)   MacEwan, S. R.; Chilkoti, A. Applications of Elastin-like Polypeptides in Drug Delivery. *J. Control. Release* **2014**, *190*, 314–330. https://doi.org/10.1016/j.jconrel.2014.06.028.

(35)   Garanger, E.; Lecommandoux, S. Emerging Opportunities in Bioconjugates of Elastin-like Polypeptides with Synthetic or Natural Polymers. *Adv. Drug Deliv. Rev.* **2022**, *191*, 114589. https://doi.org/10.1016/j.addr.2022.114589.

(36)   Weber, P.; Dzuricky, M.; Min, J.; Jenkins, I.; Chilkoti, A. Concentration-Independent Multivalent Targeting of Cancer Cells by Genetically Encoded Core-Crosslinked Elastin/Resilin-like Polypeptide Micelles. *Biomacromolecules* **2021**, *22* (10), 4347–4356. https://doi.org/10.1021/acs.biomac.1c00897.

(37)   Aruffo, A.; Stamenkovic, I.; Melnick, M.; Underhill, C. B.; Seed, B. CD44 Is the Principal Cell Surface Receptor for Hyaluronate. *Cell* **1990**, *61* (7), 1303–1313. https://doi.org/10.1016/0092-8674(90)90694-A.

(38)   Mattheolabakis, G.; Milane, L.; Singh, A.; Amiji, M. M. Hyaluronic Acid Targeting of CD44 for Cancer Therapy: From Receptor Biology to Nanomedicine. *J. Drug Target.* **2015**, *23* (7–8), 605–618. https://doi.org/10.3109/1061186X.2015.1052072.

(39)   Upadhyay, K. K.; Bhatt, A. N.; Mishra, A. K.; Dwarakanath, B. S.; Jain, S.; Schatz, C.; Le Meins, J. F.; Farooque, A.; Chandraiah, G.; Jain, A. K.; Misra, A.; Lecommandoux, S. The Intracellular Drug Delivery and Anti Tumor Activity of Doxorubicin Loaded Poly(γ-Benzyl l-Glutamate)-b-Hyaluronan Polymersomes. *Biomaterials* **2010**, *31* (10), 2882–2892. https://doi.org/10.1016/j.biomaterials.2009.12.043.

(40)   Jeannot, V.; Gauche, C.; Mazzaferro, S.; Couvet, M.; Vanwonterghem, L.; Henry, M.; Didier, C.; Vollaire, J.; Josserand, V.; Coll, J.-L.; Schatz, C.; Lecommandoux, S.; Hurbin, A. Anti-Tumor Efficacy of Hyaluronan-Based Nanoparticles for the Co-Delivery of Drugs in Lung Cancer. *J. Control. Release* **2018**, *275* (October 2017), 117–128. https://doi.org/10.1016/j.jconrel.2018.02.024.

(41)   Liu, A. Y. Expression of CD44 in Prostate Cancer Cells. *Cancer Lett.* **1994**, *76* (1), 63–69. https://doi.org/10.1016/0304-3835(94)90135-X.

(42)   Penno, M. B.; August, J. T.; Baylin, S. B.; Mabry, M.; Linnoila, R. I.; Lee, V. S.; Croteau, D.; Yang, X.

L.; Rosada, C. Expression of CD44 in Human Lung Tumors. *Cancer Res.* **1994**, *54* (5), 1381–1387.

(43) Kopp, R.; Fichter, M.; Schalhorn, G.; Danescu, J.; Classen, S. Frequent Expression of the High Molecular, 673-Bp CD44v3,v8-10 Variant in Colorectal Adenomas and Carcinomas. *Int. J. Mol. Med.* **2009**, *24* (05), 677–683. https://doi.org/10.3892/ijmm_00000279.

(44) Olsson, E.; Honeth, G.; Bendahl, P.-O.; Saal, L. H.; Gruvberger-Saal, S.; Ringnér, M.; Vallon-Christersson, J.; Jönsson, G.; Holm, K.; Lövgren, K.; Fernö, M.; Grabau, D.; Borg, Å.; Hegardt, C. CD44 Isoforms Are Heterogeneously Expressed in Breast Cancer and Correlate with Tumor Subtypes and Cancer Stem Cell Markers. *BMC Cancer* **2011**, *11* (1), 418. https://doi.org/10.1186/1471-2407-11-418.

(45) Chen, Y.; Fu, Z.; Xu, S.; Xu, Y.; Xu, P. The Prognostic Value of CD44 Expression in Gastric Cancer: A Meta-Analysis. *Biomed. Pharmacother.* **2014**, *68* (6), 693–697. https://doi.org/10.1016/j.biopha.2014.08.001.

(46) Li, X.-P.; Zhang, X.-W.; Zheng, L.-Z.; Guo, W.-J. Expression of CD44 in Pancreatic Cancer and Its Significance. *Int. J. Clin. Exp. Pathol.* **2015**, *8* (6), 6724–6731.

(47) Al-Hajj, M.; Wicha, M. S.; Benito-Hernandez, A.; Morrison, S. J.; Clarke, M. F. Prospective Identification of Tumorigenic Breast Cancer Cells. *Proc. Natl. Acad. Sci.* **2003**, *100* (7), 3983–3988. https://doi.org/10.1073/pnas.0530291100.

(48) Idowu, M. O.; Kmieciak, M.; Dumur, C.; Burton, R. S.; Grimes, M. M.; Powers, C. N.; Manjili, M. H. CD44+/CD24−/Low Cancer Stem/Progenitor Cells Are More Abundant in Triple-Negative Invasive Breast Carcinoma Phenotype and Are Associated with Poor Outcome. *Hum. Pathol.* **2012**, *43* (3), 364–373. https://doi.org/10.1016/j.humpath.2011.05.005.

(49) Prince, M. E.; Sivanandan, R.; Kaczorowski, A.; Wolf, G. T.; Kaplan, M. J.; Dalerba, P.; Weissman, I. L.; Clarke, M. F.; Ailles, L. E. Identification of a Subpopulation of Cells with Cancer Stem Cell Properties in Head and Neck Squamous Cell Carcinoma. *Proc. Natl. Acad. Sci.* **2007**, *104* (3), 973–978. https://doi.org/10.1073/pnas.0610117104.

(50) Kramer, J. R.; Petitdemange, R.; Bataille, L.; Bathany, K.; Wirotius, A. L.; Garbay, B.; Deming, T. J.; Garanger, E.; Lecommandoux, S. Quantitative Side-Chain Modifications of Methionine-Containing Elastin-Like Polypeptides as a Versatile Tool to Tune Their Properties. *ACS Macro Lett.* **2015**, *4* (11), 1283–1286. https://doi.org/10.1021/acsmacrolett.5b00651.

(51) Petitdemange, R.; Garanger, E.; Bataille, L.; Bathany, K.; Garbay, B.; Deming, T. J.; Lecommandoux, S. Tuning Thermoresponsive Properties of Cationic Elastin-like Polypeptides by Varying Counterions and Side-Chains. *Bioconjug. Chem.* **2017**, *28* (5), 1403–1412. https://doi.org/10.1021/acs.bioconjchem.7b00082.

(52) Rosselin, M.; Xiao, Y.; Belhomme, L.; Lecommandoux, S.; Garanger, E. Expanding the Toolbox of Chemoselective Modifications of Protein-Like Polymers at Methionine Residues. *ACS Macro Lett.* **2019**, *8* (12), 1648–1653. https://doi.org/10.1021/acsmacrolett.9b00862.

TABLE OF CONTENTS GRAPHIC
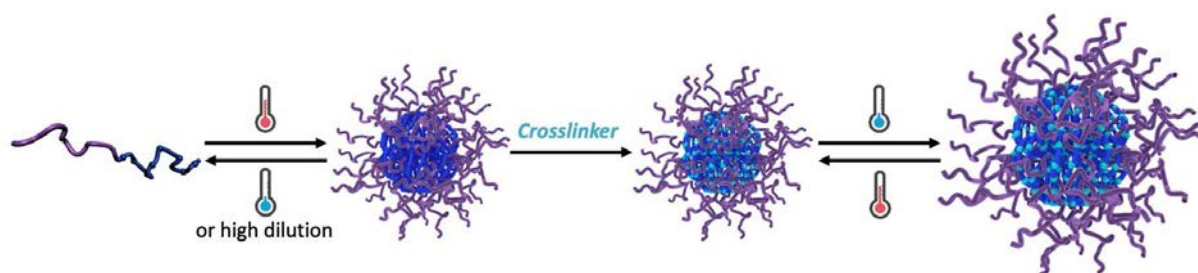
Thermoresponsive core-crosslinked nanoparticles from HA-*b*-ELP diblock copolymers

Manon Levêque,[a] Sébastien Lecommandoux,*[a] and Elisabeth Garanger*[a]

[a] Univ. Bordeaux, CNRS, Bordeaux INP, LCPO, UMR 5629, Pessac, F-33600, France.
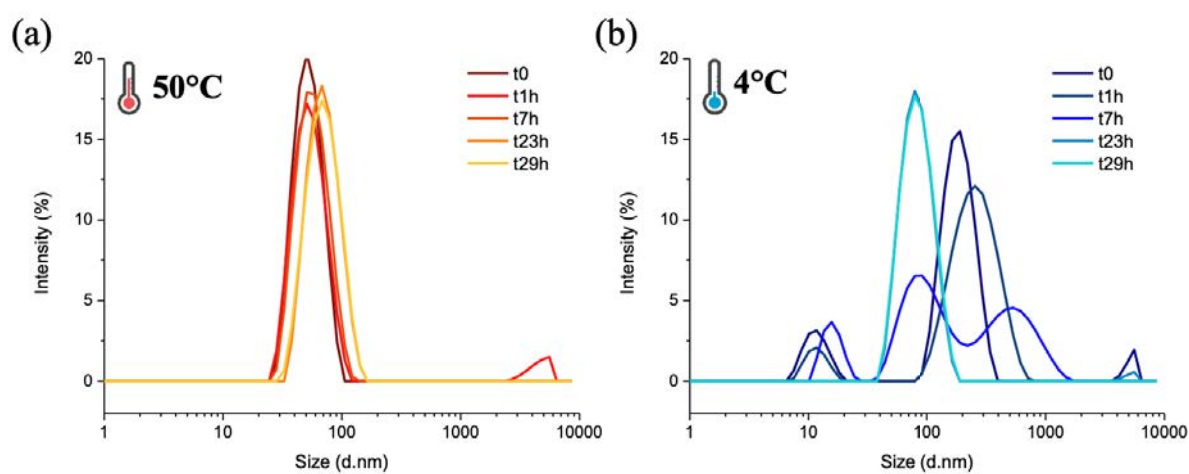
SUPPLEMENTARY FIGURES

Figure S1. Monitoring of the formation of crosslinked HA$_{4.6k}$-ELP80 nanoparticles with time during the cross-linking reaction at 50°C. DLS analysis (size distribution expressed in intensity) of the reaction mixture performed at 50°C (a) and after cooling of the sample at 4°C (b).
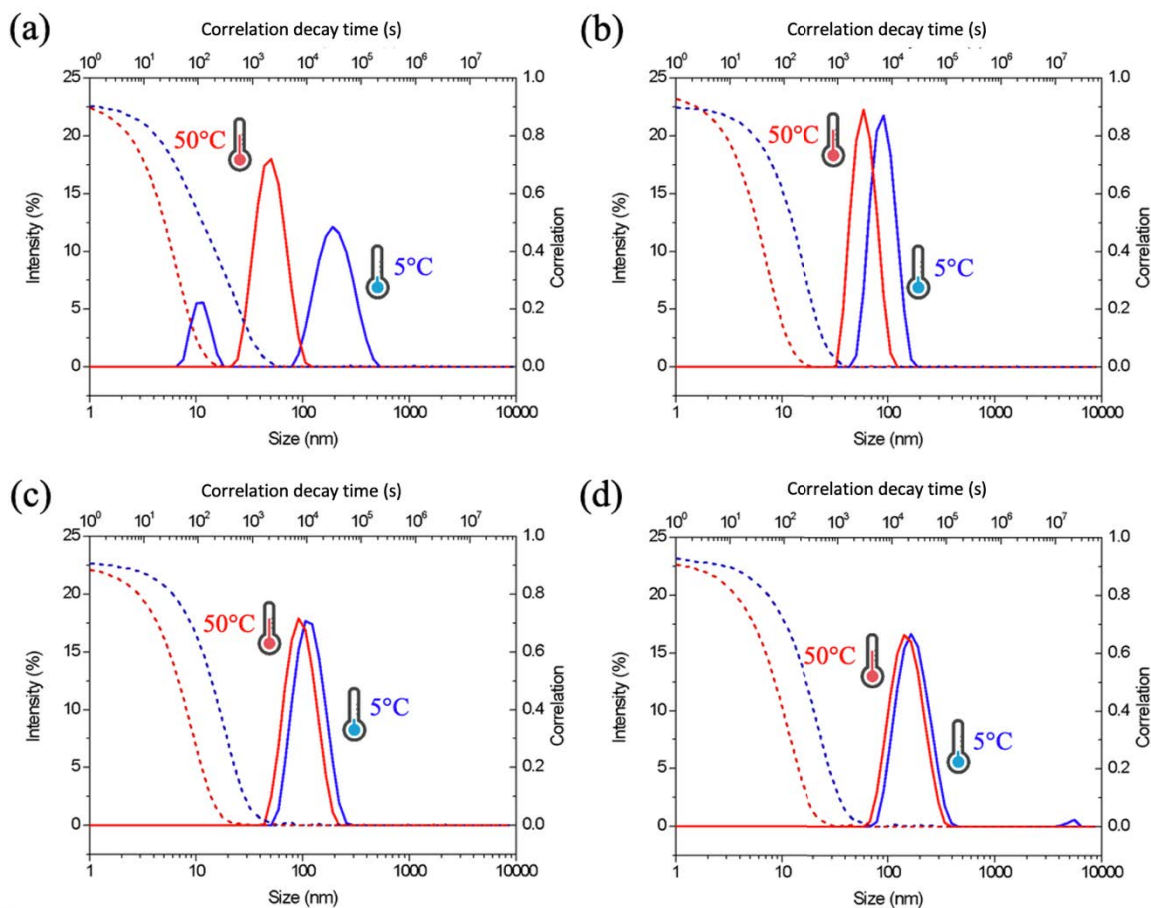
Figure S2. DLS analysis (auto-correlation functions represented as doted lines and size distributions expressed in intensity represented as solid lines) of the solution of non-crosslinked $HA_{4.6k}$-ELP80 (a) and crosslinked nanoparticles (b-d) of the three bioconjugates HA-*b*-ELP performed at 50°C and 5°C: $HA_{4.6k}$-ELP80 (b); HA_{24k}-ELP80 (c); and HA_{42k}-ELP80 (d).
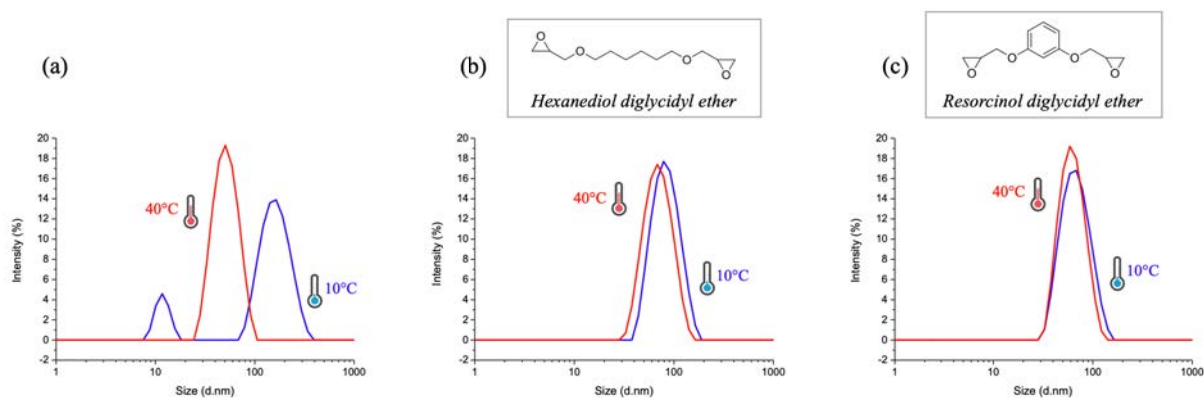

Figure S3. DLS analysis (size distribution expressed in intensity) of the solution of non-crosslinked (a) and crosslinked nanoparticles with hexanediol diglycidyl ether (b) and resorcinol diglycidyl ether (c) performed at 10°C and 50°C.
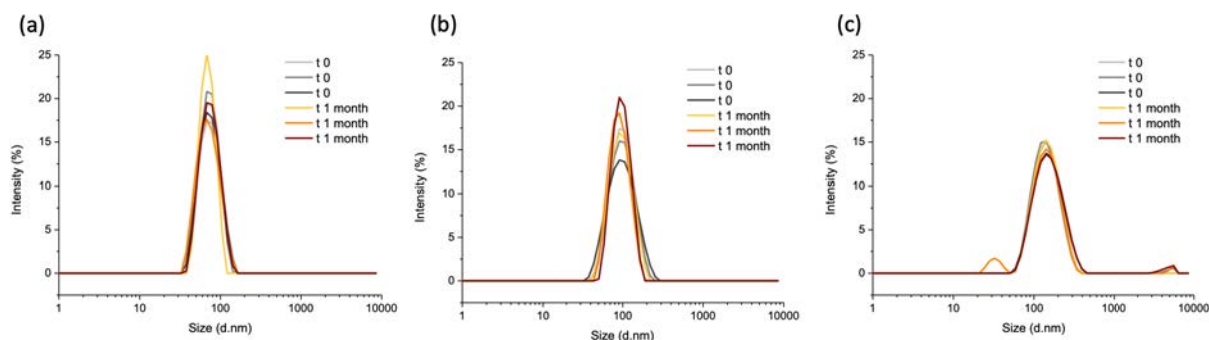
Figure S4. Stability of core-crosslinked HA-*b*-ELP[M_1V_3-80] nanoparticles in PBS after 1 month storage at 4°C. DLS analysis (size distribution expressed in intensity) performed at 4°C for (a) HA$_{4.6k}$-ELP80; (b) HA$_{24k}$-ELP80]; (c) HA$_{42k}$-ELP80. In each case, data are presented for three different nanoparticle batches.
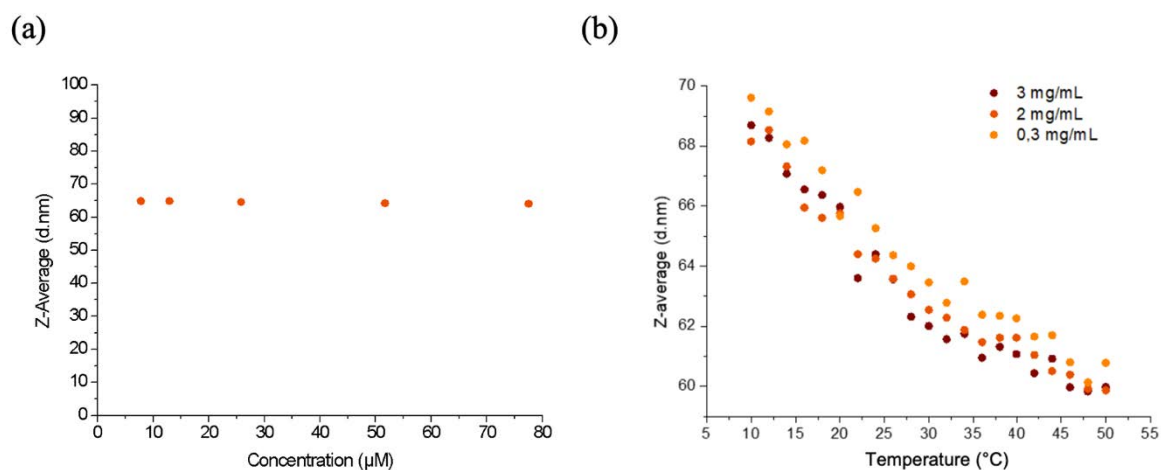

Figure S5. (a) Evolution of cross-linked HA$_{4,6k}$-ELPn80 nanoparticle size as a function of concentration (PBS, 25°C). (b) HA$_{4,6k}$-ELPn80 nanoparticle size evolution as a function of temperature and concentration.